



# Estimation of Tsunami Hazard Vulnerability Factors by Integrating Remote Sensing, GIS and AHP Based Assessment

Mohammad Reza Poursaber<sup>1,2\*</sup>, Yasuo Ariki<sup>1</sup>

<sup>1</sup>Graduate School of System Informatics, Kobe University, Kobe, Japan

<sup>2</sup>Faculty of Civil, Water and Environmental Engineering, Shahid Beheshti University, Tehran, Iran

Email: \*poursaber@me.cs.scitec.kobe-u.ac.jp

Received 16 November 2015; accepted 18 December 2015; published 29 April 2016

Copyright © 2016 by authors and OALib.

This work is licensed under the Creative Commons Attribution International License (CC BY).

<http://creativecommons.org/licenses/by/4.0/>



Open Access

## Abstract

Geographic Information Systems (GIS), image processing in remote sensing and analytical hierarchy process (AHP) were used to estimate and classify vulnerability and inundation areas under the Tohoku tsunami event 2011 in the Ishinomaki, Miyagi prefecture, Japan. Acceptable data were obtained from Geoeye-1 satellite image, GSI DEM and field survey. Five factors of elevation, slope, shoreline distance, river distance and vegetation were used to classify the vulnerability and be weighted via AHP. By assessing the estimated and classified vulnerability map and comparing it with the inundation map of the study area, we found that a 13.44 km<sup>2</sup> area came under the tsunami vulnerability zone. Inundation areas were located in high and slightly high vulnerability classifications. Kitakami river and the Unga water canal played the role of flooding strips by transporting tsunami waves into the hinterland. This research is important to understand the roles of main topographical factors in a tsunami disaster.

## Keywords

GIS, Remote Sensing, AHP and Tsunami Vulnerability Map

**Subject Areas:** Environmental Sciences

## 1. Introduction

Tsunami is a hazardous event as a natural phenomenon when happening in a populated area causes unacceptably large numbers of fatalities or property damage. By means of a vulnerable area map and performing a primary assessment, minimizing the impact of tsunami event is possible. Vulnerability is defined as an element to esti-

\*Corresponding author.

**How to cite this paper:** Poursaber, M.R. and Ariki, Y. (2016) Estimation of Tsunami Hazard Vulnerability Factors by Integrating Remote Sensing, GIS and AHP Based Assessment. *Open Access Library Journal*, 3: e2212.

<http://dx.doi.org/10.4236/oalib.1102212>

mate the disaster risk within the context of hazard and risk. Since vulnerability is a result of capacity lack, increasing in capacity means reducing vulnerability, and high vulnerability means low capacity [1] [2].

The evolution of remote sensing technology and its applications have enabled us to use satellite imagery data for mapping damage areas due to a natural disaster and also for assessing the vulnerable areas and damage distribution. As a further matter, introduction of Geographic Information System (GIS) as a database system has allowed us to analyze and display spatial data by using digitized maps for planning, mitigation and decision making [3].

GIS software with its powerful tools is widely employed by decision-makers and planners for analyzing the spatial information through spatial multi-criteria analysis. Spatial multi-criteria analysis of GIS requires standard values and geographical location features, weighted topographical factors, according to users' preferences [4]-[6]. GIS is also applicable to evaluate the strategies required for creation of coastal vegetation belts against tsunami risk and to analyze tsunami risk using a multi-scenario approach [7] [8].

Previous studies have developed and analyzed integrative remote sensing techniques in assessing building vulnerability to tsunami hazard. GIS approaches and a set of building vulnerability classification rules have been developed and successfully applied to categorize building vulnerability classes. Another study developed the Papathoma Tsunami Vulnerability Assessment (PTVA) to provide first-order assessments of building vulnerability to tsunamis. In another study to undertake assessments of coastal vulnerability, analysis data are gathered from available ASTER satellite images (Advanced Space born Thermal Emission and Reflection Radiometer) and 3s-SRTM-v3 (3 arc-seconds Shuttle Radar Topography Mission, version 3) digital elevation models which the vulnerability assessment can be displayed via GIS as a series of thematic maps. The uses of multiple geospatial variables of topographic elevation, relation to tsunami direction, coastal proximity, and coastal shape are incorporated by the Analytic Hierarchy Process (AHP) to construct a weighting scheme for the geospatial variables and assessing tsunami vulnerability [9]-[12].

## 2. Spatial Data Gathering and Analysis

In this study, remote sensing data captured by very high resolution (VHR) optical satellites with a pixel size about 0.5 meter is used to identify critical geographical elements such as buildings, transport infrastructure and possible inundation areas due to a tsunami event in order to estimate the vulnerability and risk in coastal areas. Specifically in this study, the area of Ishinomaki City in Miyagi Prefecture, (in the Tohoku region of northern Japan) was studied (**Figure 1**). Latitude and Longitude for Ishinomaki city in decimal degrees are: 38.4345°N, 141.3029°E respectively. As of September 2015, the city has an estimated population of 145,805 and a population density of 263 persons per km<sup>2</sup>. The total area was 554.50 square kilometers. Ishinomaki has a humid subtropical climate with warm summers and cold winters. These climates usually occur on the eastern coasts and eastern sides of continents like east side of Japan, from 26 to 45 latitude and it is called cfa within Köppen climate classification [13].

We extracted the factors of elevation and slope from a digital elevation model (DEM) obtained from the Geospatial Information Authority of Japan (here after referred to as GSI DEM), while the NDVI for vegetation density is extracted from Geoeye-1 image and Image Analysis toolbar in ArcGIS 10.2.1 The shoreline distance and river distance were measured from the vector maps of the study area.

The vulnerability by tsunami is then estimated by applying AHP to factors of elevation, slope, shoreline distance, river distance and vegetation. The vulnerability assessment can be displayed via GIS in terms of spatial multi-criteria analysis on a map of the tsunami vulnerability area. The general steps used in this study are shown in **Figure 2**.

### 2.1. Elevation

A digital elevation model was created from elevation data obtained from GSI (Geospatial information authority of Japan). GSI DEM was downloaded. The mesh elevation data created by interpolating to the elevation point at center point in 0.2 seconds (about 5 meter) mesh that is from the value of elevation (ground data) measured by airborne laser. The height accuracy of the 5m mesh elevation from the airborne laser is less than 0.3 m and the standard deviation of the altitude acquisition position (from the photogrammetry) is less than 1.0 meter. The data was in JPGIS (format) converted to shape file in point format using base map viewer converter software version 4.00 (FGDV) provided by GSI.

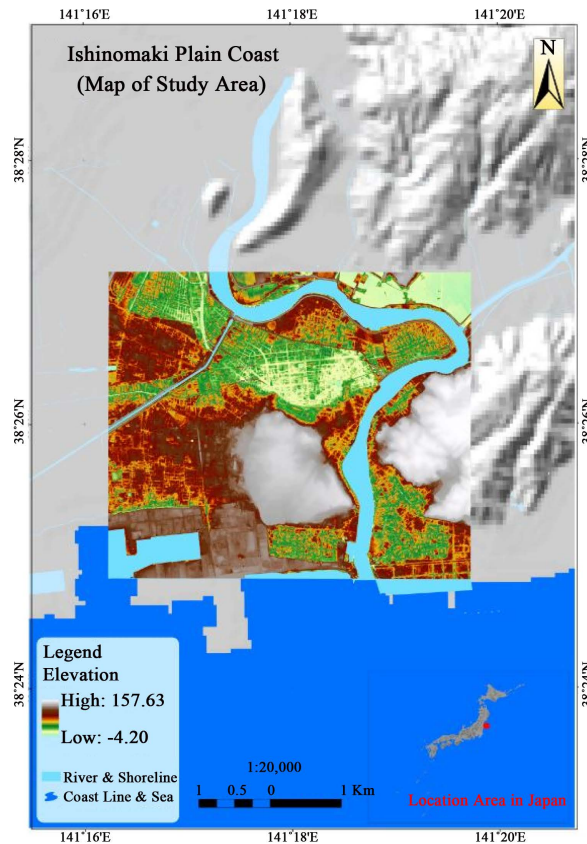


Figure 1. Case study site in Ishinomaki, Japan.

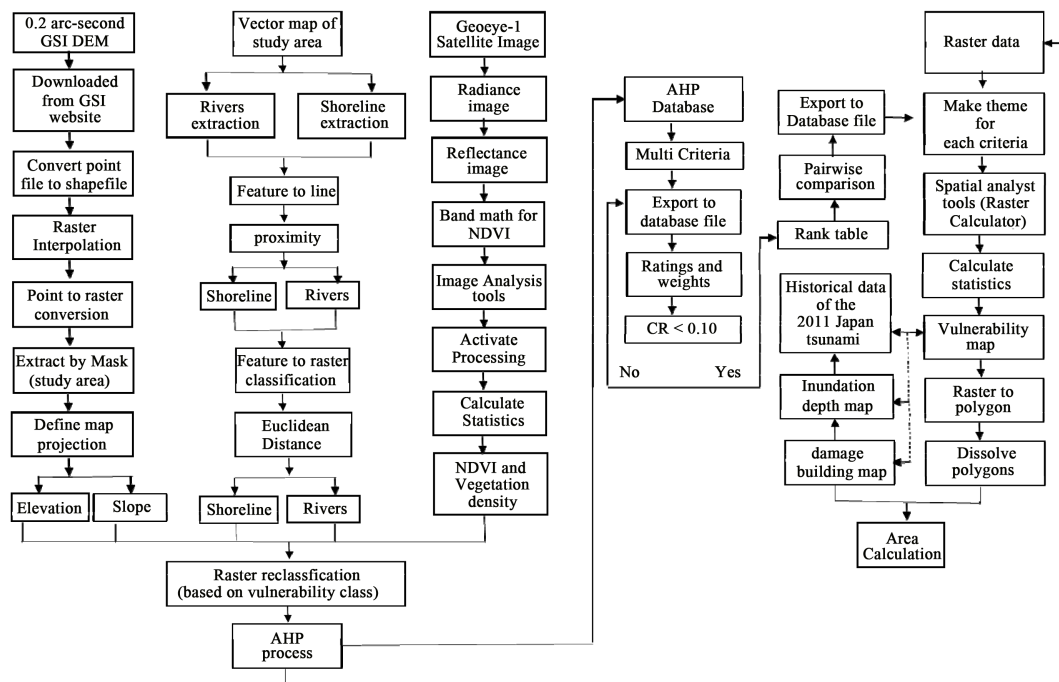


Figure 2. Framework for the study. GSI: Geospatial information authority of Japan, DEM: Digital Elevation Model, Geosy-1: Very high resolution optical satellite image, NDVI: Normalized Difference Vegetation Index, AHP: Analytical Hierarchy Process, CR: Consistency Ratio.

Finally, this point format was converted to raster for creating the digital elevation model via Arc GIS 10.2.1 software and Raster Interpolation toolset function.

## 2.2. Slope

The slope was determined as the rate of maximum change in z value from each cell of the satellite image. The use of a z-factor is essential for correct slope calculations when the surface z units are expressed in units different from the ground x, y units. The range of values in the output depends on the type of measurement units. The range of slope values is 0 to 90 for degrees and 0 to essentially infinity for percent rise. We created a slope map using the surface creation and analysis tools of the ArcGIS 10.2.1 software to use a third-order finite-difference method for calculating the slope [14].

## 2.3. Distance from Shoreline

The distance from the shoreline was created in a polyline file for buffering the distance from the shoreline to the land. We computed the distance using the proximity and the Euclidean distance analyst tool in the ArcGIS 10.2.1 software. The distance is based on the historical report of the maximum run-up in the area of study. We used Equation (1) to classify coastal proximity and shoreline distance buffering from Bretschneider and Wybro (1976) [12]:

$$\log X_{\max} = \log 1400 + \frac{4}{3} \log \left( \frac{Y_0}{10} \right) \quad (1)$$

where  $X_{\max}$  is the maximum reach of the tsunami over land, and  $Y_0$  is the tsunami height at the shore line.

The maximum run-up of the tsunami in the study area was 8.6 m according to the 2011 Tohoku Earthquake Tsunami Joint Survey Group, 2011 at Ayukawa in Ishinomaki City, Miyagi Prefecture. We classified distance buffers in five classes based on Equation (1) in order to create a tsunami vulnerability map. It explains that 4.55 m to 7.09 m of run-up can reach a distance of 489.94m from the shoreline, 7.09 m to 9.64 m of run-up can reach 885.76 m, 9.64 m to 12.18 m of run-up can reach 1332.84, 12.18 m to 14.73 m of run-up can reach 1821.46 m and 14.73 m to 17.27 m of run-up can reach more than 2345.53 m.

## 2.4. Distance from the (Kitakami) River and (Unga) Water Canal

We know the tsunami propagation in the rivers has higher speed than the tsunami propagation over land and it may maintain and propagate the wave energy further upstream and may cause damages in area far from the shoreline. The Kitakami River, the fourth largest river in Japan and the downstream branches into two water canal, Old-Kitakami river and Kitakami river. Old-Kitakami river flows on a fertile plain which has been highly developed for agriculture and industries and this water canal passes through the study area, while Kitakami river flows through a narrow valley into a small bay facing the Pacific Ocean. The Old-Kitakami river mouth had parallel jetties. The bed slope was 0.00017, which is the average bed slope from the river mouth up to the intrusion limit. On the contrary, the Kitakami river mouth was mostly sandy soil with 0.0001 bed slope and not as deep as the Old-Kitakami river mouth. It can be seen that the tsunami had reached 8 to 10 km or more off the coastline towards inland around Kitakami River and Old Kitakami River and the elevation in this region was extremely low, ranging between 0 and 2 m. while the devastated damages to the building were seen till the 3 km of the river area while the inundation area was about 8 km in the study area [15] [16].

Kitakami-unga or Kitakami Canalis an artificial watercourse (canal) with an average elevation of 9 meter below sea level along 15.8 km. The soil in the area is high in andosols (an), soils composed of volcanic materials, usually dark colored. Kitakami Canal ran across the city and then inundated the inland area. Similarly to the river study, based on the historical report of the inundation area and inundation depth maps, we evaluated the inundated area along the water canal. Accordingly the influence of water canal width on the inundation flows was classified into three classes which are shown in Figure 7.

The elevation, river distance and shoreline distance were classified into five classes of vulnerability using the Jenks natural breaks method. This classification method indicates by picking the class breaks in best group similar values, maximize the differences between classes and minimize value differences between data within the same class and emphasize the differences between the reclassified classes [17]. The tsunami vulnerability map based on the elevation, slope, shoreline distance, river distance and Unga canal distance are shown in Figure 3-7.

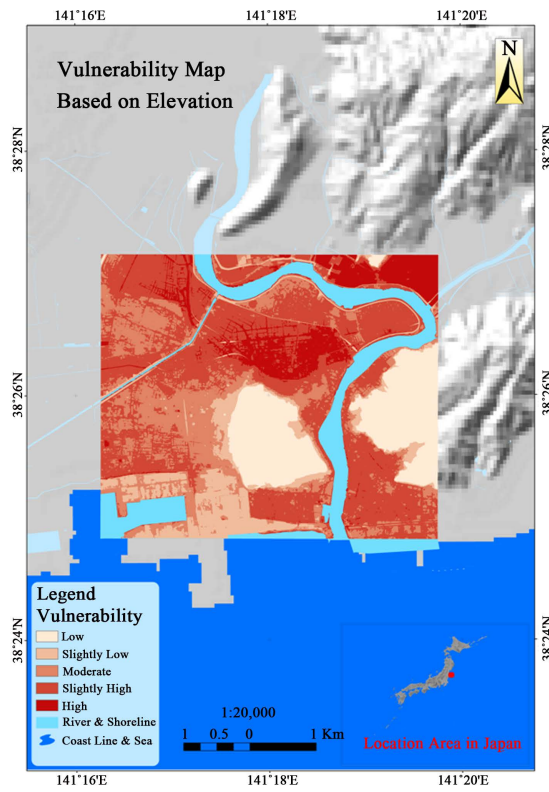


Figure 3. Vulnerability map based on elevation.

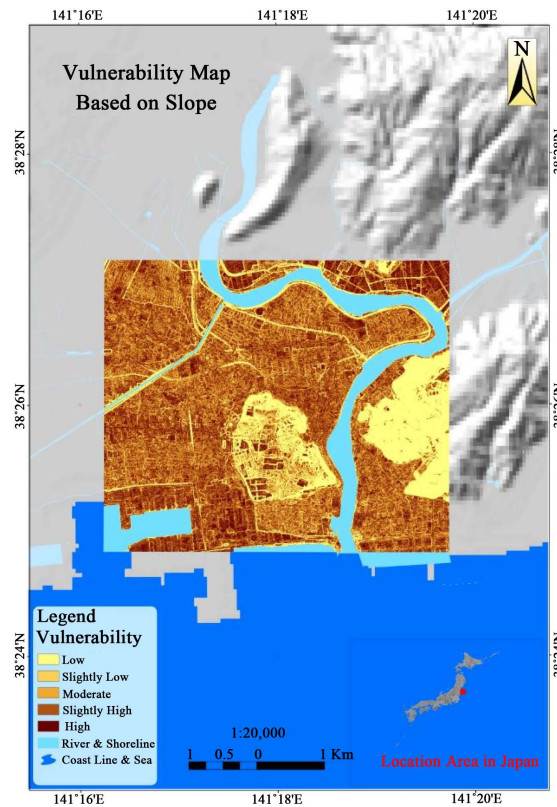


Figure 4. Vulnerability map based on slope.

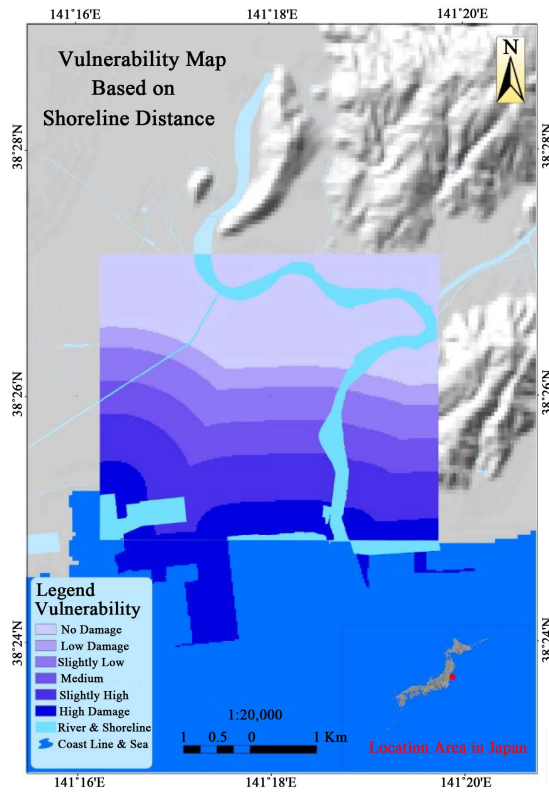


Figure 5. Vulnerability map based on shoreline distance.

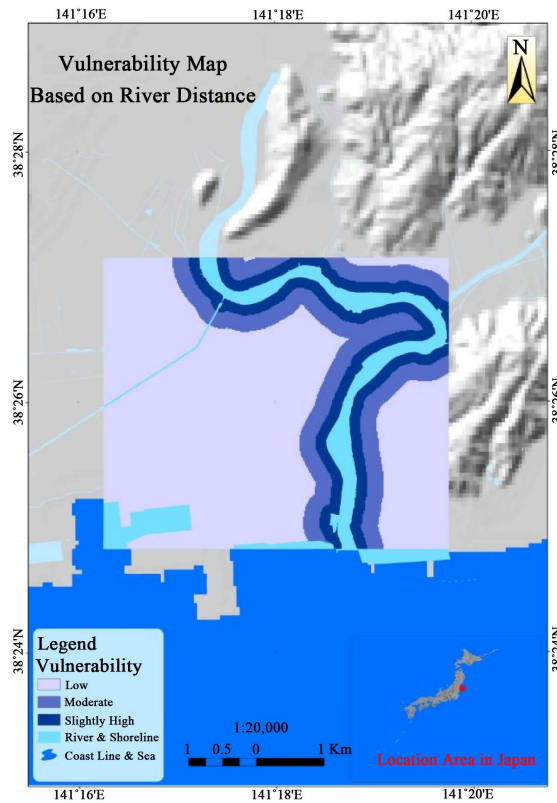


Figure 6. Vulnerability map based on river distance.

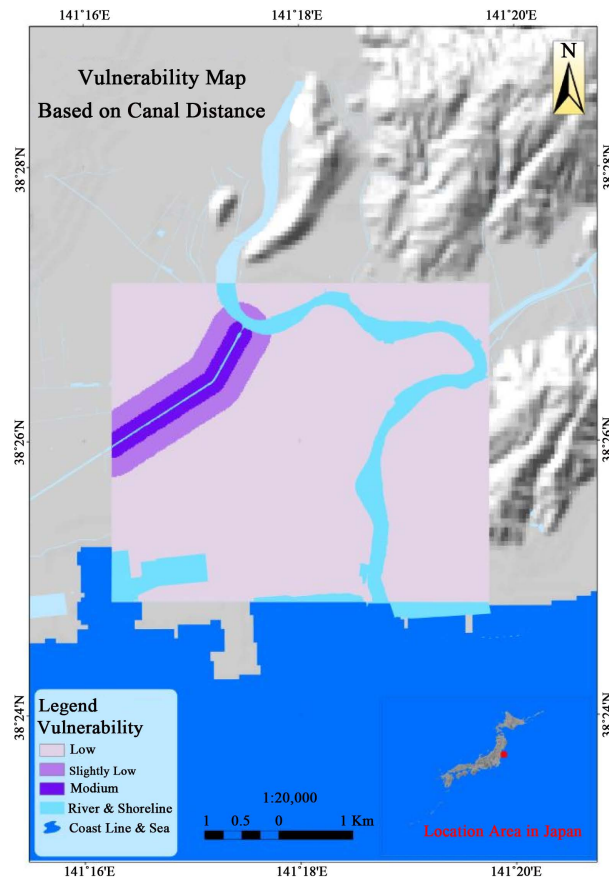


Figure 7. Vulnerability map based on the Canal distance.

### 3. GeoEYE-1 Processing

We calculated normalized difference vegetation index (NDVI), and vegetation density by using GeoEye-1 satellite image. The spectral radiance can be calculated from the digital number (DN) values in the GeoEye-1 image product using the radiometric gain and offset values in the product metadata by Equation (2) and the steps to create vegetation density map are described in the following subsection:

#### 3.1. Conversion of DN to Radiance

Equation (2) describes the algorithm for converting DN to radiance:

$$L_{\lambda} = \text{Gain}_{\lambda} \cdot \text{DN}_{\lambda} + \text{Offset}_{\lambda} \quad (2)$$

In which,

$\lambda$  = Specific spectral band of image: Near-IR, Red, Green, Blue or Panchromatic;

$L_{\lambda}$  = Spectral radiance for band  $\lambda$  at the sensor's aperture ( $\text{mW}/\text{cm}^2/\mu\text{m}/\text{str}$ );

$\text{Gain}_{\lambda}$  = Radiometric calibration gain ( $\text{mW}/\text{cm}^2/\mu\text{m}/\text{str}/\text{DN}$ ) for band  $\lambda$  from product metadata;

$\text{DN}_{\lambda}$  = Digital number values for band  $\lambda$  of image product;

$\text{Offset}_{\lambda}$  = Radiometric calibration offset ( $\text{mW}/\text{cm}^2/\mu\text{m}/\text{str}$ ) for band  $\lambda$  from product metadata [18].

The bandwidths for the GeoEye-1 bands are given in Table 1, which are calculated by integrating over the relative spectral response curve of each band filter.

#### 3.2. Conversion Radiance to Reflectance

Equation (3) describes the converting from radiance to reflectance [18].

**Table 1.** GeoEye-1 band-dependent factors.

GeoEye-1 Band ( $\lambda$ )	spectral response for each band	
	Bandwidth ( $\mu\text{m}$ )	$E_{\text{sun}\lambda}$ ( $\text{mW}/\text{cm}^2/\mu\text{m}$ )
Blue	0.0584	196.0
Green	0.0646	185.3
Red	0.0316	150.5
Near IR	0.1012	103.9

$$\rho_p = \frac{\pi \cdot L_\lambda \cdot d^2}{E_{\text{sun}\lambda} \cdot \cos \theta_s} \quad (3)$$

$\theta_s = 90^\circ$ -Solar Elevation Angle (from metadata).

where,

$\rho_p$  = Unitless planetary reflectance;

$d$  = Earth-Sun distance (astronomical units) from nautical handbook;

$E_{\text{sun}\lambda}$  = Mean solar exoatmospheric spectral irradiances ( $\text{mW}/\text{cm}^2/\mu\text{m}$ ), at an Earth-Sun distance of one astronomical unit (A.U.);

$\theta_s$  = Solar zenith angle in degrees, (The solar zenith angle is calculated from the solar elevation angle);

$L_\lambda$  = Spectral radiance for band  $\lambda$  at the sensor's aperture ( $\text{mW}/\text{cm}^2/\mu\text{m}/\text{str}$ ).

### 3.3. NDVI and Vegetation

The Normalized Difference Vegetation Index (NDVI) is a common tool for identifying and characterizing vegetation and a measure of the difference in reflectance between these wavelength ranges that takes values between  $-1$  and  $1$ , while vegetated areas produce values starting around  $0.4$  and approaching  $1.0$  and values  $<0$  indicating no vegetation [19].

Equation (4) was used for NDVI calculation and specification:

$$\text{NDVI} = \frac{(\text{NIR} - \text{RED})}{(\text{NIR} + \text{RED})} \quad (4)$$

In which for GeoEye-1 Band 4 is NIR (near infrared band) and Band 3 is red.

We classified elevation and the distance for river, canal and shoreline based on the values described in **Table 2**.

As shown in **Figure 8**, a vulnerability map based on vegetation density, explained that most of high-vulnerability areas were located in the coastal areas where the vegetation is less.

## 4. GIS and AHP for Vulnerability Mapping

Cell-based modeling in spatial analysis was used to specify the vulnerability area due to tsunami hazard. Cells are classified into five classes of vulnerability in the numbers of 1, 2, 3, 4 and 5, which represent low, slightly low, medium, slightly high, and high vulnerability classes.

AHP is a multi-criteria decision-making analysis (MCDA) approach introduced by Saaty (1977, 1980), which is developed by a series of pair-wise comparisons between each factor relative to other factors to make a scaled set of preferences. By the AHP measurement theory, pair wise comparisons and relies on the judgments of experts to conclude (derive) priority scales that measure intangibles in relative terms. The AHP is an Eigen value technique to the pair-wise comparisons approach and a numerical fundamental scale, which ranges from 1 to 9 to calibrate the quantitative and qualitative performances of priorities to score the importance of each factor (Saaty, 2008). **Table 3** describes the fundamental scale of absolute numbers which is named the Saaty nine-point comparison scale. As we mentioned each number explains (depends on) the relative importance of each factor [20].

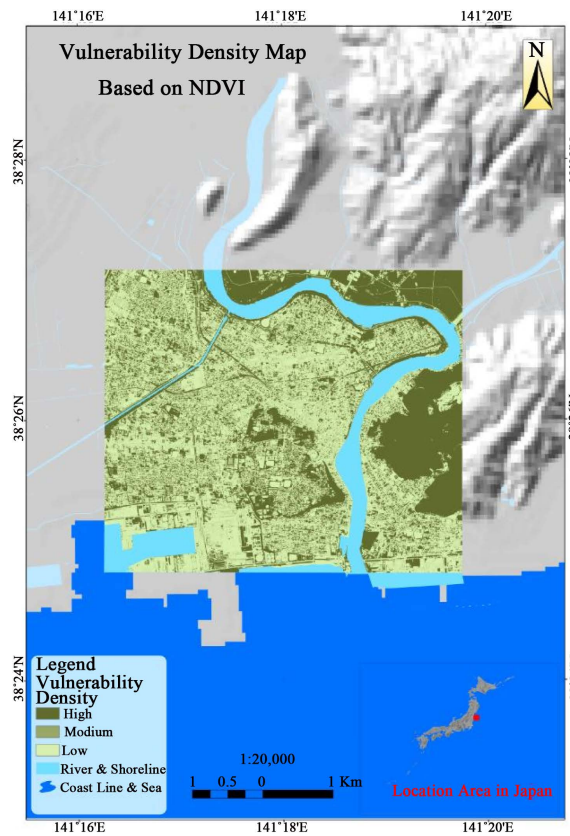


Figure 8. Vulnerability map based on vegetation density.

Table 2. Tsunami vulnerability classes based on elevation, Shoreline distance, river distance and vegetation.

Vulnerability class	Factors name						
	Elevation (m)	Slope (%)	Shoreline distance (m)	River distance (m)		Vegetation	
				Kitakami	Unga canal	Index	Density
High (5)	-4 - -3	0 - 1	0 - 489.94	-	-	-0.998 - 0.151	Low
Slightly high (4)	3 - 4	1 - 3	489.94 - 1198.53	-	-	0.151 - 0.164	Slightly low
Medium (3)	4 - 5	3 - 6	1198.53 - 1700.48	0 - 160	1 - 150	0.164 - 0.188	Medium
Slightly low (2)	5 - 6	6 - 8	1700.48 - 2184.28	160 - 400	150 - 400	0.188 - 0.218	Slightly high
Low (1)	>6	>8	2184.28 - 2491.91	>680	>400	0.218 - 0.556	High

Table 3. The saaty nine-point comparison scale [21].

Intensity of importance (Score)	Definition and Explanation	
	Definition	Explanation
1	Equal importance	Two factors contribute equally to the objective
3	Weak importance of one over another	The judgment is slightly favor one factor over another
5	Essential or strong importance	The judgment is to strongly favor one factor over another
7	Demonstrated importance	A factor is strongly favored and its dominance is demonstrated in practice
9	Absolute importance	The evidence favoring one factor over another is of the highest possible order of affirmation
2, 4, 6, 8	Intermediate values between the two adjacent judgments	When compromise is needed

All of tsunami vulnerability factors are overlaid and weighted based on their dominant influences in determining the class of tsunami vulnerability. The relative importance of each factor within the hierarchy is determined by their weights (Saaty, 1977 & 1980) with a pair wise comparison as shown in **Table 4**. The hierarchical interactions based on the respective importance of each factor were computed by estimating the numerical score. When there are evaluation criteria/objectives, decision makers must carry out a pairwise comparison. The scores are made by the subjective definition of the investigator in determining the importance of each factor [22].

The first eigenvector computed based on the pairwise comparison matrix shown in **Table 4**, an approximation of Eigen vector (and Eigen value) of a reciprocal matrix can be obtained by or through the following method: 1) sum of each column of the reciprocal matrix; 2) Then we divide each element of the matrix with the sum of its column, we have normalized relative weight where the sum of each column is 1 as shown in **Figure 9**. The normalized principal Eigen vector can be obtained by averaging across the rows. The normalized principal eigenvector explains that shoreline distance has the highest weight (42.16%), followed by elevation (14.92%), slope (8.57%), river distance (26.60%) and vegetation density (7.74%) as shown in **Figure 9**.

AHP is subjective and tolerates inconsistency through the amount of redundancy by providing a measure of inconsistency assessment, which is shown by consistency ratio (CR). If the value of Consistency Ratio is smaller or equal to 10%, the inconsistency is acceptable. CR indicates the probability that the matrix judgments were randomly generated and it is defined as the ratio of the consistency index (CI), which is the degree of logical consistency among pair-wise comparisons, to the random consistency index (RI) which is the average CI value of randomly-generated comparison matrices.

Equations (5) and Equation (6) describe the algorithms for CR and CI calculation:

$$CR = \frac{CI}{RI} \tag{5}$$

$$CI = \frac{\lambda_{max} - n}{n - 1} \tag{6}$$

In which:

$\lambda_{max}$  is the maximum eigenvalue of the judgment matrix and calculated from the sum of all factors and is multiplied by its eigenvector which is 42.16%;

$n$  is the size of the comparison matrix. In this study,  $n = 5$ .

The RI is based on the random consistency index as shown in **Table 5**. The RI of 1.11 was used for five factors of normalized matrix in **Figure 10**.

So the consistency index, CI, is calculated 0.093 and CR is 8.37%.

Elevation	0.1429	0.1818	0.1460	0.1224	0.1538	14.92%
Slope	0.0714	0.0909	0.1095	0.0816	0.0769	8.57%
Shoreline distance	0.4286	0.3636	0.4380	0.4898	0.3846	42.16%
River distance	0.2857	0.2727	0.2190	0.2449	0.3077	26.60%
Vegetation	0.0714	0.0909	0.0876	0.0612	0.0769	7.74%

**Figure 9.** Normalized matrix and eigenvector calculation.

**Table 4.** Pairwise comparison.

Pairwise Comparison	Factors Name				
	Elevation	Slope	Shoreline Distance	River Distance	Vegetation
Elevation	1.00	2.00	0.33	0.50	2.00
Slope	0.50	1.00	0.25	0.33	1.00
Shore-Line Distance	3.00	4.00	1.00	2.00	5.00
River Distance	2.00	3.00	0.50	1.00	4.00
Vegetation	0.50	1.00	0.20	0.25	1.00

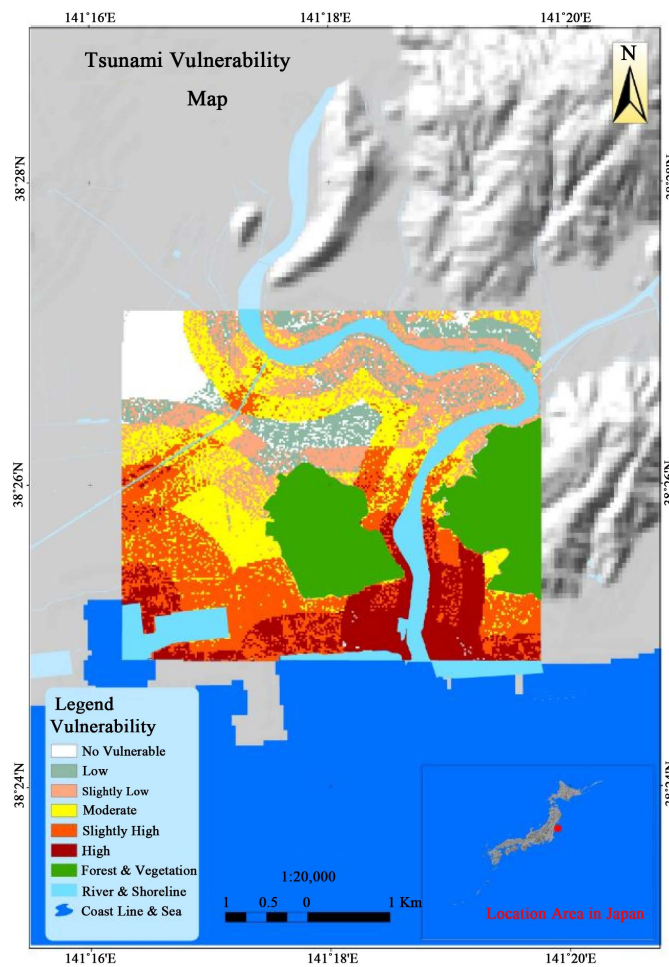


Figure 10. Tsunami vulnerability map of Ishinomaki Study area.

Table 5. Value of the Random Index (RI) [23].

Random Consistency Index	Matrix Size									
	1	2	3	4	5	6	7	8	9	10
RI	0.00	0.00	0.52	0.89	1.11	1.25	1.35	1.40	1.45	1.49

We calculated each raster cell-by-cell basis of the factor to its weight. A Weighted Linear Combination (WLC) analysis is very straightforward in a raster GIS, and the factors that are being utilized are combined by applying a weight, to each followed by a summation of the results to proceed a suitability map. Equation (7) describes the suitability calculation [19] [20] and [23]:

$$S = \sum W_i \cdot X_i \tag{7}$$

where:

$S$  = Suitability;

$W_i$  = Weight of factor  $i$ ;

$X_i$  = the criterion score of factor  $i$  (potential rating of the factor).

We estimated raster calculator in map algebra menu using the spatial analyst tools of ArcGIS 10.2.1 to produce vulnerability map by applying Equations (7).

Figure 10 shows the tsunami vulnerability map in the Ishinomaki area as output of this calculation. We estimated the statistics of the vulnerability map based on the vulnerability classification of five factors used in this

study is shown in **Table 6** while the vulnerability index of 91,437.35 grid cells ranged between 1 to 5, with a standard deviation of 0.792. The GIS produced tsunami vulnerability map is shown in **Figure 10** which is in good agreement with the historical data recorded by “GSI” and “2011 Earthquake Tsunami Joint Survey Group”. Based on the comparison most of the inundation areas are located in high and slightly high vulnerability areas.

Based on the result of our study, which is shown in **Figure 11** the inundation area was 14.14 km<sup>2</sup>, while GSI reported that the inundation area in Ishinomaki in the 2011 Japan tsunami was 13.44 km<sup>2</sup>. On the study area the maximum inundation height (run-up) based on the 2011 Earthquake Tsunami Joint Survey Group was 8.6 m and found at Ayukawa in Ishinomaki City, Miyagi Prefecture.

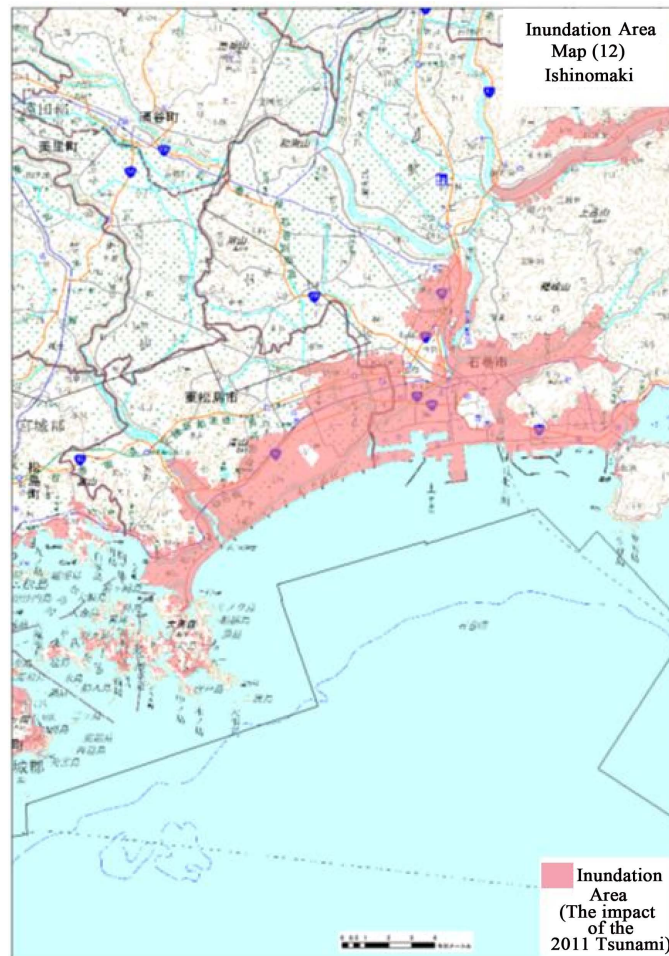


**Figure 11.** Tsunami Impact map in Ishinomaki (published by GSI) [24].

**Table 6.** Vulnerability classification and tsunami inundated area.

Vulnerability index	Vulnerable Area Classification			
	Vulnerability class	Vulnerability Value in Tsunami Map	Area (km <sup>2</sup> )	Area (%)
5	High	3.45 - 4.73	2.432	17.20
4	Slightly high	2.85 - 3.45	3.747	26.50
3	Medium	2.28 - 2.85	3.146	22.25
2	Slightly low	1.84 - 2.28	3.235	22.88
1	Low	1.57 - 1.84	1.579	11.17

## 5. Discussion

Vulnerability is defined as the potential area that can be damaged by natural hazards. Physical vulnerability is often defined as the loss degree to a given factor or set of factors within the area affected by a hazard like tsunami. Physical factors, such as elevation, slope, shoreline distance, river distance and vegetation density could be used for vulnerability classification. Moreover, we know “Inundation” is the result of a tsunami traveling a long distance inland and is a horizontal measurement of the path of the tsunami. A tsunami effect is defined by several factors like height, run-up height and run-up distance [25]-[27].

In this research, we used and analyzed satellite remote sensing (data), elevation data and field survey data followed by multi-criteria analysis through AHP raster overlay tools in GIS processing can be used as the basic operation for vulnerability mapping and inundation assessment due to tsunami hazard.

In this study a first attempt for assessing tsunami vulnerability was performed by using the factor of river distance besides elevation, vegetation, shoreline distance and slope and applying the AHP method combined with raster overlay tools through GIS processing in the Ishinomaki area. It is valuable step to estimate inundation area via this method and primary tsunami vulnerability mapping for impact assessment and output.

Remote sensing can be capable to achieve information about the input factors for tsunami vulnerability mapping and impact assessment. In the study area, several indicators of vulnerability can be achieved using a very high resolution satellite. It is very useful to derive data about the DEM in high spatial resolution so the output of the research will result in higher accuracy. Although obtaining the digital elevation model from GSI DEM needs some processing and ArcGIS is a powerful software for processing and combining spatial data of each factor and analyzing the result of AHP in order to generate a vulnerability map.

In this study, we used five classes of vulnerability for tsunami vulnerability map. Based on this, 2.432 km<sup>2</sup> of the study area was in high vulnerability, 3.747 km<sup>2</sup> was in slightly high vulnerability, 3.146 km<sup>2</sup> was in medium vulnerability, 3.235 km<sup>2</sup> was in slightly low vulnerability and 1.579 km<sup>2</sup> of the area was in low vulnerability. The high-vulnerability areas were located in the coastal areas in low slopes. In high-vulnerability area and slightly high vulnerability inundation areas were predicted. In addition, the Kitakami River and water canal have the role to act as a flooding strip that transports inundation into the hinterland. The tsunami run-up comes up to the hinterland through the flat surface, urban areas and rivers. In this research we created the tsunami vulnerability map and inundation map which can be used for determining the priority for land-use planning related to tsunami hazard risk management.

In this research, we proposed the combined analysis of digital elevation data, very high resolution satellite images, tsunami historical data, AHP, and spatial multi-criteria processing via GIS to provide a tsunami vulnerability map and inundation map. Using the reflectance value of Geoeye-1 image before and after 2011 Japan, Tohoku tsunami was calculated as a preliminary study. In the next research, the height of the buildings and their materials in the inundation area can be considered in classifying the damaged buildings.

## 6. Conclusions

In recent years, vulnerable areas due to tsunami disaster have been studied by means of GIS application on satellite images and AHP method used in multi-criteria analysis. By means of GIS application, it is possible to manage hazards due to tsunami disasters. In the case of data limitation, very high resolution of the DEM and other factors, such as coastal type, relative direction of tsunami, coastal bathymetry and river morphological consideration is needed to achieve a better tsunami vulnerability mapping.

In this study, we proposed five factors in order to create a tsunami vulnerability map in accordance with the inundation area map of tsunami in Ishinomaki area of Miyagi Prefecture in Japan. As a result of this vulnerability map, although the importance of the shoreline areas in the creation of whole inundation pattern is observed, our results indicate an important role of rivers in inundation pattern far from the coast line. Furthermore, low level land areas far from the coast line are observed to be in inundated areas. The simulated tsunami pattern shows over eighty percent compatible with the inundation map.

This study used high resolution of DEM for the input factors of elevation and slope. We also calculated NDVI for the factor of vegetation index by using Geoeye-1 satellite image and the NDVI button on the Image Analysis window in the Arc GIS software.

In conclusion, by using multiple geospatial variables of topographic elevation, relation to tsunami direction, coastal proximity, and coastal shape incorporated by the AHP, an appropriate pair-wise comparison of AHP is

proposed to construct a weighting scheme for the geospatial variables and assessing tsunami vulnerability.

Our research can be employed to evaluate the assessment of the vulnerable areas that could be affected by tsunami hazard in future natural disasters.

## Acknowledgements

The technical and financial supports by Research Center for Urban Safety and Security (RCUSS) of Kobe University and Shahid Beheshti University are gratefully acknowledged. Authors are thankful to the GSI for providing DEM data and vector maps of the study area and 2011 Tohoku Earthquake Tsunami Joint Survey for the survey data in the study area.

## References

- [1] Department of Regional Development and Environment Executive Secretariat for Economic and Social Affairs Organization of American States (1991) Primer on Natural Hazard Management in Integrated Regional Development Planning. Washington DC.
- [2] Roxana, L., Ciurean, D.S. and Glade, T. (2013) Conceptual Frameworks of Vulnerability Assessments for Natural Disasters Reduction. INTECH Published, 1-32.
- [3] FEMA (2015) Applications of GIS for Emergency Management, Lesson 1: Introduction and Course Overview, IS-922. Accessed on 16 August 2015. <https://emilms.fema.gov/is922/GISsummary.htm>
- [4] Stephen, J.C. (2007) Integrating Multi-Criteria Evaluation with Geographical Information Systems. *Geographical Information Systems*, **5**, 321-339.
- [5] Islam, T. and Saman, S. (2006) Spatial Information-Based Approach for Integrated Coastal Resource Management in Asian Tsunami-Affected Countries. FAO Regional Office Asia and Pacific, The Regional Workshop on Information Management and Coordination Mechanisms of Tsunami Emergency and Rehabilitation Operations in Agriculture, Fisheries and Forestry, 287-311.
- [6] James, C.A., Harriet, D.R., Hoag, D.L., McMaster, G.S., Vandenberg, B.C., Shaffer, M.J., Wetz, M.A. and Ahjua, L.R. (2002) Multi-Criteria Spatial Decision Support Systems: Overview, Applications, and Future Research Directions. 175-180.
- [7] Deichmann, U., Ehrlich, D., Small, C. and Zeug, G. (2011) Using High Resolution Satellite Data for the Identification of Urban Natural Disaster Risk. European Union and World Bank.
- [8] Sambah, A.B. and Miura, F. (2013) Remote Sensing, GIS, and AHP for Assessing Physical Vulnerability to Tsunami Hazard. World Academy of Science, Engineering and Technology. *International Journal of Environmental, Ecological, Geological and Mining Engineering*, **7**.
- [9] für Geowissenschaften, F. (2010) Assessing Building Vulnerability to Tsunami Hazard Using Integrative Remote Sensing and GIS Approaches. Dissertation Thesis.
- [10] Dall'Osso, F., Gonella, M., Gabbianelli, G., Withycombe, G. and Dominey-Howes, D. (2009) A Revised (PTVA) Model for Assessing the Vulnerability of Buildings to Tsunami Damage.
- [11] Dall'Osso, F., Bovio, L., Cavalletti, A., Immordino, F., Gonella, M. and Gabbianelli, G. (2010) A Novel Approach (the CRATER Method) for Assessing Tsunami Vulnerability at the Regional Scale Using ASTER Imagery. *Italian Journal of Remote Sensing*, **42**, 55-74.
- [12] Sinaga, T.P.T., Nugroho, A., Lee, Y.-W. and Suh, Y. (2010) GIS Mapping of Tsunami Vulnerability: Case Study of the Jembrana Regency in Bali, Indonesia.
- [13] National Oceanic and Atmospheric Administration (2012) Ishinomaki Climate Normals 1961-1990.
- [14] Weih Jr., R.C. and Mattson, T.L. (2004) Modeling Slope in a Geographic Information System. *Journal of the Arkansas Academy of Science*, **58**, 100-108.
- [15] Tanaka, H., Kayane, K., Adityawan, M.B. and Farid, M. (2013) The Effect of Bed Slope to the Tsunami Intrusion into Rivers. *Coastal Dynamics*, 1601-1610.
- [16] Adityawan, M.B., Roh, M., Tanaka, H. and Farid, M. (2012) The Effect of River Mouth Morphological Features on Tsunami Intrusion. 75-83.
- [17] Campbell, J.E. and Shin, M. (2012) Geographic Information System Basics. v. 1.0, Chap. 6, 133-163.
- [18] Podger, N.E., Colwell, W.B. and Taylor, M.H. (2011) GeoEye-1 Radiance at Aperture and Planetary Reflectance.
- [19] (2002) 3.3 Normalised Difference Vegetation Index (NDVI). NDVI: A Non-Technical Overview.
- [20] Singh, S.K., Chandel, V., Kumar, H. and Gupta, H. (2014) RS & GIS Based Urban Land Use Change and Site Suita-

- bility Analysis for Future Urban Expansion of Parwanoo Planning Area, Solan, Himachal Pradesh (India). *International Journal of Development Research*, **4**, 1491-1503.
- [21] Saaty, T.L. (1977) A Scaling Method for Priorities in Hierarchical Structures. *Journal of Mathematical Psychology*, **15**, 234-281. [http://dx.doi.org/10.1016/0022-2496\(77\)90033-5](http://dx.doi.org/10.1016/0022-2496(77)90033-5)
- [22] Teknomo, K. (2006) Analytic Hierarchy Process (AHP).
- [23] Rao, R.V. (2013) Decision Making in the Manufacturing Environment Using Graph Theory and Fuzzy Multiple Attribute Decision Making Methods, Chapter 2, Improved Multiple Attribute Decision Making Methods. <http://www.springer.com/978-1-4471-4374-1>
- [24] Geospatial Authority of Japan (GSI) (2015) Map of Inundation Area Due to the 2011 Great East Japan Earthquake, Map Number 12. Accessed on 2 November 2015. <http://www.gsi.go.jp/common/000059847.pdf>
- [25] Chandrasekar, N., Immanuel, J.L., Sahayam, J.D., Rajamanickam, M. and Saravanan, S. (2007) Appraisal of Tsunami Inundation and Run-Up along the Coast of Kanyakumari District, India—GIS Analysis. *Oceanologia*, **49**, 397-412.
- [26] Gencer, E.A. (2013) Natural Disasters, Urban Vulnerability, and Risk Management: A Theoretical Overview. In: Gencer, E.A., Ed., *The Interplay between Urban Development, Vulnerability, and Risk Management*, Mediterranean Studies, Vol. 7, Chap. 2, Springer-Verlag, Berlin, 7-43.
- [27] Papathoma-Köhle, M., Ulbrich, T., Keiler, M., Pedoth, L., Totschnig, R., Glade, T., Schneiderbauer, S. and Eidswig, U. (2014) Vulnerability to Heat Waves, Floods, and Landslides in Mountainous Terrain: Test Cases in South Tyrol. In: Birkmann, J., Kienberger, S. and Alexander, D., Eds., *Assessment of Vulnerability to Natural Hazards: A European Perspective*, Elsevier Publications, Amsterdam, 179-201. <http://dx.doi.org/10.1016/b978-0-12-410528-7.00008-4>